

Discovery of a monoclonal, high-affinity CD8+ T cell clone following natural hepatitis C virus infection

Curtis Cai¹, Elizabeth Keoshkerian², Kristof Wing³, Jerome Samir⁴, Manuel Effenberger³, Kilian Schober⁵, Rowena Bull⁶, Andrew Lloyd¹, Dirk Busch⁷, and Fabio Luciani¹

¹UNSW

²The Kirby Institute

³Technical University of Munich

⁴UNSW Sydney

⁵Friedrich-Alexander-Universität Erlangen-Nürnberg

⁶University of New South Wales School of Medical Sciences

⁷Technische Universität München

April 12, 2024

Abstract

CD8+ T cells recognising their cognate antigen are typically recruited as a polyclonal population consisting of multiple clonotypes with varying T-cell receptor (TCR) affinity to the target peptide-MHC (pMHC) complex. Advances in single-cell sequencing have increased accessibility towards identifying TCRs with matched antigens. Here we present the discovery of a monoclonal CD8+ T cell population with specificity for a hepatitis C virus (HCV)-derived HLA class I epitope (HLA-B*07:02 GPRLGVRAT) which was isolated directly ex vivo from an individual with an episode of acutely resolved HCV infection. This population was absent prior to infection and underwent expansion and stable maintenance for at least two years after infection as measured by HLA-multimer staining. Furthermore, the monoclonal clonotype was characterised by an unusually long dissociation time (half-life = 794 seconds and $k_{off} = 5.73 \times 10^{-4}$) for its target antigen when compared to previously published results. A comparison with related populations of HCV-specific populations derived from the same individual and a second individual suggest that high-affinity TCR-pMHC interactions may be inherent to epitope identity and shape the phenotype of responses which has implications for rational TCR selection and design in the age of personalised immunotherapies.

INTRODUCTION

The diversity and functionality of CD8+ T cells recruited during an epitope-specific response is thought to arise through the contribution of antigen density¹, antigen sensitivity², TCR gene biases³, and other factors, but the precise contributions are incompletely understood. There are further constraints which shape the diversity of the final repertoire based on structural features at key conserved residues⁴ and consideration of a T-cell clone's pre-existing frequency in the naïve repertoire^{5,6} although this may be overcome by repeated antigen re-exposure through vaccination⁷. Typically, these factors conspire to generate epitope-specific responses consisting of a range of unique TCR arrangements (clonotypes)⁸, with a distinct affinity for their cognate peptide in the context of MHC (pMHC). Notably however, epitope-specific populations have been observed to comprise few or single unique clonotypes during infection with human immunodeficiency virus⁹ and *Mycobacterium tuberculosis*¹⁰. Such monoclonal populations may have arisen through a selective advantage intrinsically conferred by its specific TCR clonotype.

The affinity of the TCR-pMHC interaction may be measured by both its association (k_{on}) and dissociation (k_{off}) constants, which collectively contribute to its host cell's activation potency¹¹. One such method for

the measurement of the k_{off} rate utilises dissociable HLA multimers, so-called MHC Streptamers, which allow the real-time tracking of dissociation of monomeric TCR-pMHC complexes by flow cytometry¹²⁻¹⁴. Notably, CD8⁺ T cell clonotypes with lower k_{off} constants (or practically, high-affinity clones with extended dissociation times) have improved protective capacity when used for adoptive transfer¹³ and high affinity neoantigen-specific clones are more effective at slowing tumor growth¹⁵. By contrast, low-affinity clonotypes are preferentially expanded long-term during chronic cytomegalovirus infection¹⁶, may be better suited for providing responses optimised against antigens with relatively higher abundance¹⁷, and provide the flexibility for recognising and responding to mutated epitopes¹⁸. Taken together, these studies provide evidence that the affinity of TCR-pMHC interactions likely influence the functional capacity of epitope-specific populations.

In this study, we characterised the phenotype and affinity of a naturally-derived monoclonal CD8⁺ T cell population arising from an individual with acutely resolving infection that we had reported on previously¹⁹. We examined three hepatitis C virus (HCV)-specific CD8⁺ T cell populations from two individuals and profiled each population's respective repertoire diversity, phenotypic characteristics, and dissociation affinities at the single-cell level. The k_{off} rate-derived affinity of the monoclonal TCR clonotype was the strongest out of all tested sequences, although clonotypes from a polyclonal population targeting the same epitope also displayed surprisingly strong affinities. Notably, analysis of the transcriptional signatures from each population revealed associations between epitope specificity, affinity and molecular phenotype. Our findings contribute to an improved understanding of the heterogeneity of TCR repertoires generated by viral infections and offer insights into how affinity may shape the phenotype and expansion of T cells at the epitope-specific level.

RESULTS

We selected three epitope-specific populations of CD8⁺T cells from two individuals (CL-MCRL and CL-3089) with acutely resolving HCV infection for this study. Both individuals were selected from a cohort of high-risk injecting drug users followed prospectively for recent HCV infection^{19,20}. CL-MCRL experienced a brief period of acute HCV infection (Figure 1A) that was bound by negative HCV RNA PCR tests at 80 days before and 115 days after the estimated date of infection²¹. Similarly, we identified a single time point for individual CL-3089 at 180 days post-infection (DPI) with a positive HCV RNA PCR test. Two peripheral HCV-specific CD8⁺ T cell populations were identified from CL-MCRL targeting the HLA-B*07:02 *GPRLGVRAT* (GPR) and HLA-A*01:01 *ATDALMTGF* (ATD) epitopes whilst a single population targeting the HLA-B*07:02 *GPRLGVRAT* epitope was identified from CL-3089 (Table 1).

We stained for epitope-specific populations using MHC-I Dextramers and flow cytometry (Figure 1B) and tracked the stable persistence of the GPR-specific population from CL-MCRL over at least two years (Figure 1C). We applied TCR reconstruction from single-cell RNA-sequencing using the VDJPuzzle pipeline²² and found that the GPR-specific population from CL-MCRL consisted almost completely of a monoclonal population of CD8⁺ T cells expressing an identical paired CDR3 $\alpha\beta$ clonotype across all four sampled time points (Figure 1D). More specifically, this monoclonal clonotype (TCR α : CAVRATGQNFVF, TCR β : CASSQAPPQGVDIQYF) accounted for 171/174 of all reconstructed paired CDR3 $\alpha\beta$ clonotypes from the GPR-specific population from CL-MCRL. By comparison, the ATD-specific and GPR-specific CD8⁺ T cell populations from individuals CL-MCRL and CL-3089, respectively, were highly diverse and polyclonal (Supplementary Figure 1). Notably, we did not observe the monoclonal GPR clonotype from CL-MCRL in the repertoire derived from CL-3089. Taken together, these observations point to the expansion of a naturally-occurring monoclonal population following natural HCV infection.

We next explored whether the recruitment and expansion of a monoclonal population may have been driven by the affinity characteristics of the monoclonal TCR for its cognate peptide target. To this end, we employed the use of reversible MHC Streptamers¹⁴ to measure the dissociation time of the TCR-pMHC interaction and determine its k_{off} affinity (Figure 1E). Briefly, reversible Streptamers were formed from conjugating fluorescently labelled pMHC monomers with a Strep-Tactin backbone via Strep-tag binding sites, and the addition of biotin dissociates the backbone by competitive binding and leaves monomeric TCR-pMHC complexes. The dissociation speed of monomeric TCR-pMHC complexes can subsequently be measured and

corresponds to the k_{off} rate. We applied this assay directly to cryopreserved peripheral blood mononuclear cells (PBMC) from CL-MCRL by first co-staining with reversible Streptamers and non-reversible Dextramers for the GPR-epitope (Figure 1F). Following the addition of biotin, we observed rapid loss of the backbone signal (half-life: 26 seconds) and gradual loss of pMHC signal (Figure 1G). We periodically paused acquisition to preserve sample during the extended dissociation between the monoclonal TCR population GPR-epitope presented on pMHC complexes, and after analysis determined the dissociation to have a half-life of 794 seconds and a k_{off} constant of 1.3×10^{-3} (95% confidence interval: 1.5×10^{-3} to 1.1×10^{-3}).

We were unable to directly measure the k_{off} affinities of the polyclonal populations from CL-MCRL and CL-3089 because of the breadth of unique TCR arrangements, and thus we applied an *in vitro* colony expansion approach to generate pure, monoclonal populations of epitope-specific CD8⁺ cells from single-cell sorted cells. Single clones from the GPR- and ATD-specific populations from CL-MCRL and CL-3089 respectively, were identified by staining with non-reversible Dextramers, isolated by fluorescence-activated cell sorting, and expanded by stimulation with phytohemagglutinin (PHA) and IL-2, in the presence of gamma irradiated feeder cells for 4 weeks (Table 1). We also applied this approach to the monoclonal GPR-specific population from CL-MCRL and successful expansions typically yielded up to one million CD8⁺ T cells. We next repeated the dissociation assay using these colony expanded cells by first re-identifying epitope-specific cells by non-reversible multimer staining (Figure 2A and Methods) followed by measurement of reversible Streptamer dissociation comprising of the backbone (Figure 2B) and pMHC complex (Figure 2C).

Notably, the dissociation half-life varied in duration between colonies, epitope specificity, and individual origin. The strongest k_{off} affinity was recorded from CL-MCRL GPR-specific colonies (half-lives 1039 to 1321 seconds), followed by CL-3089 GPR-specific colonies (half-lives 247 to 1191 seconds), and the weakest k_{off} affinities were recorded from CL-MCRL ATD-specific colonies (half-lives 22 to 196 seconds) (Figure 2D). More specifically, the k_{off} constants for the CL-MCRL ATD-specific colonies ranged from 3.54×10^{-3} to 3.14×10^{-2} (Table 2), the k_{off} constants for the CL-MCRL GPR-specific colonies ranged from 5.25×10^{-4} to 6.67×10^{-4} (Table 3), and the k_{off} constants for the CL-3089 GPR-specific colonies ranged from 5.82×10^{-4} to 2.81×10^{-3} (Table 3). Intriguingly for one pair of colonies (F4 and F4-2) derived from the polyclonal GPR-specific population, their dissociation half-lives were within the range of the monoclonal clonotype (Table 3) which suggested that it may be possible to identify similarly high affinity TCRs within polyclonal populations.

Our sorting strategy for colony expansion resulted in the random selection of clonotypes and thus we performed targeted TCR sequencing to link clonotype identity with measured k_{off} affinities. Total RNA was extracted from a subset of samples and the CDR3 regions from TCR α and TCR β chain transcripts were enriched by nested PCR followed by Sanger sequencing. All ATD-specific colonies had distinct clonotypes (Table 2), which was consistent with the polyclonal nature of the original repertoire (Supplementary Figure 1). Notably, around half of all clonotypes from the colony expansions had also been observed in the scRNA-seq dataset (Tables 2 and 3).

Finally, we considered whether, at the population level, transcriptional phenotypes may be associated with differences in the distribution of k_{off} affinities. We first performed a differential gene expression analysis between the GPR- and ATD-specific populations from the early time points (<120 days post-infection) in CL-MCRL and identified enrichment for effector-associated signatures (*NKG7*, *GZMH*, *GZMA*) in the former and a memory-associated signature (*IL7R*) in the latter (Figure 3A). Next, we compared the GPR-specific monoclonal population from CL-MCRL and the polyclonal one from CL-3089, but identified differences primarily related to TCR gene usage and mitochondrial gene expression which may reflect inter-individual differences (Figure 3B). Rather, the GPR population from CL-3089 resembled an intermediate population between the ATD- and GPR-specific populations when characterised by expression for the phenotypic markers *NKG7*, *GZMH*, and *IL7R* (Figure 3C). We further applied gene set enrichment analysis using Hallmark pathways from the Molecular Signatures database which confirmed that the GPR-specific population exhibited an effector-polarised phenotype with evidence for elevated cell cycling and cellular metabolism pathways in its enriched genes (Figure 3D and E). Taken together, our findings suggest an association between affinity and transcriptional phenotype at the population level whereby higher affinity

responses can also be observed in combination with highly active effector phenotypes.

DISCUSSION

During a typical CD8⁺ T cell immune response, a range of clonotypes are recruited, each with their own distinct affinity for the target epitope. In this study we identified an HCV-specific clonotype from an individual with acutely resolved infection that was monoclonal expanded and exhibited a strong affinity for the HLA-B*07:02 *GPR* epitope, with a dissociation rate significantly smaller than the ones of previously reported TCRs^{13,14}. Intriguingly, a polyclonal repertoire from a second individual that also generated a response against the same epitope also exhibited similar dissociation rates, suggesting that affinity alone may not be a sufficient factor regulating whether monoclonal or polyclonal populations arise.

Our findings provide evidence that high-affinity TCRs may be more common than previously observed, or particular epitopes may bias the recruitment of higher affinity receptors. Previous studies of TCR dissociations using the same assay have reported half-lives typically of up to 200 seconds^{13,14,23}, which was exceeded by all GPR-specific clonotypes in this study.

The affinity between a TCR and its target pMHC is particularly meaningful for dictating the activation potency of CD8⁺ T cell clones²⁴ which may have contributed to the accelerated differentiation and expansion of the monoclonal GPR-specific clonotype at the expense of recruitment of additional clonotypes. It is plausible that the range of affinities measured from our colony expansions may have been biased to favour subsets such as central memory T cells which have greater capacity for clonal expansion *in vitro* by cytokine stimulation²⁵ or high affinity clonotypes which are more responsive to memory recall responses^{26,27}.

The role of affinity in determining T cell fate remains unclear, with contrasting reports on the role of high affinity in driving memory T cell fate²⁸⁻³⁰. High-affinity clones were found dominating during the acute phase of infection, while under chronic conditions, low-affinity repertoires may be favoured through mechanisms such as mutational escape epitopes upon viral evolution or re-infection¹⁸. Our new study is consistent with a model that high-affinity memory cells can be detected in the acute phase of viral infection, and these are phenotypically and transcriptionally distinct from effector cells that contribute to IFN- γ production¹⁹. In this study we studied high-risk behaviour individuals who inject drugs, thus it is likely that continuous exposure to HCV may contribute to the formation of memory populations, and therefore to future protective immunity^{31,32}. Nevertheless, more studies are needed to dissect the role of affinity in determining the fate of a cytotoxic T cell response³³ and whether the affinity profile of memory populations continue to be shaped by future antigen encounter.

Our findings will benefit the growing field of personalized immunotherapies involving the rational TCR design. Notably, rational engineering of the monoclonal receptor offers the possibility to further enhance its affinity, for example to synthesize specific high-affinity TCRs against neoantigen targets³⁴.

CONCLUSION

In summary, this study expanded the known range of k_{off} rates and provided a collection of TCR sequences which may have application for comparative studies between high and low affinity receptors.

METHODS

Study subjects

Two individuals with acutely resolving HCV infection (CL-MCRL and CL-3089) were sourced from the HITS cohort (reference) for single-cell RNA-sequencing (scRNA-seq). For each population, cells from a single timepoint following resolution of infection were selected for sorting cells for single-cell colony expansion.

Single-cell RNA-sequencing

scRNA-seq was performed as described previously¹⁹. Briefly HCV-specific CD8⁺ T cell populations were isolated by HLA-I Dextramer staining (HLA-A*01:01 *ATDALMTGF* or HLA-B*07:02 *GPRLGVRAT*) (Immudex) and sorting with flow cytometry (BD FACSAria III) for plate-based Smart-Seq2 scRNA-seq^{35,36}.

Sequencing was performed with 150bp paired end sequencing on Illumina NovaSeq 6000 and NextSeq 500 platforms. Full length TCR sequences were reconstructed using the VDJpuzzle package with default parameters ²².

Reversible and non-reversible multimer preparation

Reversible MHC Streptamers were prepared by incubating 1 μ g of the relevant pMHC monomer conjugated to AF488 (HLA-B*07:02 *GPRLGVRAT* or HLA-A*01:01 *ATDALMTGF*) (laboratory synthesis) with 1 μ g Strep-Tactin-APC (IBA Lifescience, PN 6-5010-001) in 25 μ l of FACS buffer (PBS/1% BSA). Non-reversible multimers were similarly prepared by incubating 1 μ g of the relevant pMHC monomer conjugated to biotin (laboratory synthesis) with 1 μ g of Streptavidin-PE (BioLegend, PN 405245). Incubations were performed on ice in the dark for 45 minutes. Streptamers and multimers were used within 6 hours of preparation.

K_{off} dissociation assay using PBMC

The dissociation rate for the GPR-specific population from CL-MCRL was measured directly from cryopreserved PBMC. Cryopreserved cells were thawed and stained first with the reversible Streptamer for 20 minutes followed by surface antibody staining: CD8-eFluor450 (OKT-8) and CD19-PE-Cy5 (HIB19) for an additional 20 minutes without washing. Cells were then washed twice and stained with a HLA-B*07:02 *GPRLGVRAT* Dextramer (Immudex, Copenhagen, Denmark) for 20 minutes. Two final washes were performed, and cells were resuspended with one drop of propidium iodide (Molecular Probes) and 100 μ l of FACS buffer. Data was acquired on a LSR Fortessa x20 (BD Biosciences) in a cooled tube holder. After a brief period of acquisition, a 1X biotin solution (Sigma-Aldrich) was added to dissociate the reversible Streptamer. Additional biotin solution was added as required and the tube containing cells was periodically placed on ice without sample acquisition to preserve sample availability during the dissociation process. The time between subsequent acquisitions was embedded in raw FCS files and used to determine the time since initial acquisition.

Single-cell colony expansion

Total PBMC were thawed and stained first with the relevant Dextramer conjugated to PE (Immudex), followed by Fixable yellow viability stain (Invitrogen) and finally a panel of surface antibodies: CD3-BV480 (UCHT1), CD8-APC-R700 (RPA-T8), CD19-PE-Cy5 (HIB19). Single HCV-specific CD8⁺ T cells (lymphocytes/singlets/live cells/CD3⁺/CD19⁻/CD8⁺/Dextramer⁺) were sorted into separate wells of a 384-well flat bottom plate containing expansion media (CTS OpTmizer T Cell Expansion serum free media) (Gibco) supplemented with L-glutamine (2mM) (Sigma-Aldrich), penicillin/streptomycin (1X) (Sigma-Aldrich), IL-2 (500IU/ml) (STEMCELL Technologies), PHA-L (1 μ g/ μ l) (Sigma-Aldrich) and containing 1 \times 10⁶ gamma irradiated feeder PBMC cells from unrelated blood donors. Sorting was performed with single cell precision on a FACS Aria III flow cytometer (BD) and plates were incubated in a 37°C, 5% CO₂ incubator.

On day 7 after sorting, 50 μ l of supplementing media containing CTS OpTmizer T Cell Expansion serum free media with L-glutamine (2 mM), penicillin/streptomycin (1X concentration), and IL-2 (500 IU/ml) was added to each well. On every subsequent 3-4 days, 50 μ l of existing media was removed and replaced with an equal volume of supplementing media. If cell colonies reached 100% confluency, they were transferred to 96-well flat bottom plates (typically after three weeks) in supplementing media containing PHA-L (1 μ g/ μ l). Colonies continued to be monitored and supplemented every 3-4 days and after an additional two weeks or when 100% confluency was reached, they were cryopreserved in two identical aliquots containing 50% media, 40% FBS, and 10% DMSO.

K_{off} dissociation assay using colony expansions

Single-cell expansions were retrieved from cryopreservation and stained first with the reversible Streptamer for 20 minutes followed by surface antibody staining: CD8-eFluor450 (OKT-8) and CD19-PE-Cy5 (HIB19) for an additional 20 minutes without washing. Cells were then washed twice and stained with the non-reversible multimer for 20 minutes. Two final washes were performed, and cells were resuspended with one drop of propidium iodide (molecular probes) and 100 μ l of FACS buffer.

Data acquisition by flow cytometry for dissociation assay

Stained cells were transferred to 5 mL round-bottom polystyrene tubes which had been pierced with a syringe to allow delivery of a biotin solution during acquisition. Cells were kept cool at 4°C or on ice at all points during preparation and acquisition. Data were acquired on an LSR Fortessa x20 (BD Biosciences). At the beginning of data acquisition, events were recorded for up to 60 seconds followed by rapid injection of 1.5 mL PBC containing 1X biotin (Sigma-Aldrich). Samples were continuously acquired until loss of MHC monomer signal was observed and additional biotin solution was added as required.

Calculation of dissociation and k_{off} constants

Compensated fluorescence and time values from the lymphocyte/singlet/live/CD8+/non-reversible multimer subpopulation were exported from raw FCS files using FlowJo (v10.6.1, BD) and loaded into Prism (v7.04, GraphPad). Time values (in seconds), MHC-AF488, and Strep-Tactin-APC fluorescence values were used as input for non-linear regression under ‘XY analyses’ to compute the half-life values for the associated dissociation curve. k_{off} values were calculated by taking the reciprocal of the computed half-life in seconds and upper and lower 95% confidence intervals for half-lives were also reported.

Targeted TCR amplification of colony expansions

Total RNA was extracted from an aliquot of cells from selected single-cell colony expansions using an RNeasy micro kit (Qiagen) and stored at -20°C. RNA was reverse transcribed using the SuperScript IV Reverse Transcriptase kit (Invitrogen) according to manufacturer’s recommendations. First, template RNA was incubated with a poly dT primer (AAGCAGTGGTATCAACGCAGAGTACT₃₀VN) and nucleotides for 5 minutes at 65°C then immediately placed on ice. Next, the mix containing reverse transcriptase and buffer was added and the mixture was incubated at 50°C for 15 minutes followed by 80°C for 10 minutes.

Two rounds of nested PCRs were performed to enrich for TCR-associated transcripts using previously published primer pools³⁷. All reactions used identical cycling conditions consisting of an initial denaturation (95°C for one minute) followed by 35 cycles of: 95°C for 20 seconds, 52°C for 20 seconds, 72°C for 45 seconds, followed by a final extension at 72°C for 4 minutes. For the first round PCR, alpha and beta chain transcripts were amplified in a single reaction consisting of PCR buffer (1X), dNTPs (0.2 mM), TRAC external primer (0.4 µM), TRBC external primer (0.4 µM), TRAV external primer pool (0.1 µM), TRBV external primer pool (0.1 µM), Taq DNA polymerase (Qiagen), and 5ul of reverse transcribed template. For the second round nested PCR, 2.5 µl of first round product was added to a total reaction mix of 25 µl containing PCR buffer (1X), dNTPs (0.2mM) and Taq DNA polymerase (Qiagen). Separate reactions were prepared for the amplification of alpha and beta chain transcripts containing either TRAC internal primer (0.4 µM) and TRAV internal primer pool (0.1 µM), or TRBC internal primer (0.4 µM) and TRBV internal primer pool (0.1 µM).

Amplification products were validated by gel electrophoresis and purified using ExoSAP-IT Express (Applied Biosystems). Samples were submitted for Sanger sequencing at the UNSW Ramaciotti Centre for Genomics using the relevant internal constant region primer. Electropherograms after sequencing were manually inspected for clear signals. Nucleotide sequences were used to query the online IMGT/V-QUEST tool and obtain TCR gene usage and CDR3 amino acid sequences (available at http://www.imgt.org/IMGT_vquest/input).

ACKNOWLEDGEMENTS

We thank the study participants for their generous donation of samples. The HITS-p investigators include Andrew Lloyd, Lisa Maher, Kate Dolan, Paul Haber, William Rawlinson, Carla Treloar and Gregory Dore. This research was supported from National Health and Medical Research Council of Australia (NHMRC) Project Nos. APP1121643, 1027551, 1060199, Partnership No. 1016351, and Programme Nos. 510488 and 1053206. The HITS-c cohort was supported by the UNSW Hepatitis C Vaccine Initiative and NHMRC Project Grant No. 630483. F.L., A.R.L. and R.A.B. are supported by NHMRC Research Fellowships (Numbers: 1128416, 1041897 and 1084706). F.L., A.R.L. and R.A.B. are supported by NHMRC

Research Fellowships (Numbers: 1128416, 1041897 and 1084706). C.C. and J.S. are supported by Australian Government Research Training Program (RTP) Scholarships. D.H.B. was supported by the Deutsche Forschungsgemeinschaft (DFG, SFB-TRR338/1-452881907-A01). K.S. is supported by the German Federal Ministry of Education and Research (BMBF, projects 01KI2013). The authors acknowledge the facilities and technical support from the staff at the UNSW Flow Cytometry core facility located within the Mark Wainwright Analytical Centre. Sequencing was performed by staff at the Ramaciotti Centre for Genomics, UNSW. Analyses of single-cell sequencing data were performed with resources allocated from the National Computational Infrastructure, Australia.

AUTHOR CONTRIBUTIONS

Curtis Cai : Data curation, formal analysis; investigation; methodology; writing – original draft. **Jerome Samir** : Data curation; formal analysis. **Elizabeth Keoshkerian** : Investigation; methodology. **Kristof Wing** : Formal analysis; investigation; methodology. **Manuel Effenberger** : Investigation. **Kilian Schober** : Investigation. **Rowena A Bull** : Investigation. **Andrew R Lloyd** : Investigation. **Dirk H Busch** : Conceptualization; investigation. **Fabio Luciani** : Conceptualization; data curation; formal analysis; funding acquisition; investigation; methodology; project administration; supervision; writing – review and editing.

CONFLICT OF INTEREST

All the other authors declare no conflict of interest related to this work.

REFERENCES

- 1 Bullock, T. N., Mullins, D. W. & Engelhard, V. H. Antigen density presented by dendritic cells in vivo differentially affects the number and avidity of primary, memory, and recall CD8+ T cells. *J Immunol* **170** , 1822-1829 (2003). <https://doi.org/10.4049/jimmunol.170.4.1822>
- 2 Almeida, J. R. *et al.* Antigen sensitivity is a major determinant of CD8+ T-cell polyfunctionality and HIV-suppressive activity. *Blood* **113** , 6351-6360 (2009). <https://doi.org/10.1182/blood-2009-02-206557>
- 3 Miles, J. J., Douek, D. C. & Price, D. A. Bias in the alphabeta T-cell repertoire: implications for disease pathogenesis and vaccination. *Immunol Cell Biol* **89** , 375-387 (2011). <https://doi.org/10.1038/icb.2010.139>
- 4 Dash, P. *et al.* Quantifiable predictive features define epitope-specific T cell receptor repertoires. *Nature* **547** , 89-93 (2017). <https://doi.org/10.1038/nature22383>
- 5 Obar, J. J., Khanna, K. M. & Lefrancois, L. Endogenous naive CD8+ T cell precursor frequency regulates primary and memory responses to infection. *Immunity* **28** , 859-869 (2008). <https://doi.org/10.1016/j.immuni.2008.04.010>
- 6 Schulien, I. *et al.* Characterization of pre-existing and induced SARS-CoV-2-specific CD8(+) T cells. *Nat Med* **27** , 78-85 (2021). <https://doi.org/10.1038/s41591-020-01143-2>
- 7 Qi, Q. *et al.* Diversification of the antigen-specific T cell receptor repertoire after varicella zoster vaccination. *Sci Transl Med* **8** , 332ra346 (2016). <https://doi.org/10.1126/scitranslmed.aaf1725>
- 8 Chen, G. *et al.* Sequence and Structural Analyses Reveal Distinct and Highly Diverse Human CD8(+) TCR Repertoires to Immunodominant Viral Antigens. *Cell Rep* **19** , 569-583 (2017). <https://doi.org/10.1016/j.celrep.2017.03.072>
- 9 Kalams, S. A. *et al.* Longitudinal analysis of T cell receptor (TCR) gene usage by human immunodeficiency virus 1 envelope-specific cytotoxic T lymphocyte clones reveals a limited TCR repertoire. *J Exp Med* **179** , 1261-1271 (1994). <https://doi.org/10.1084/jem.179.4.1261>
- 10 Hodapp, T. *et al.* Massive monoclonal expansion of CD4 T-cells specific for a Mycobacterium tuberculosis ESAT-6 peptide. *Eur Respir J* **40** , 152-160 (2012). <https://doi.org/10.1183/09031936.00175611>

- 11 Aleksic, M. *et al.* Dependence of T cell antigen recognition on T cell receptor-peptide MHC confinement time. *Immunity* **32** , 163-174 (2010). <https://doi.org/10.1016/j.immuni.2009.11.013>
- 12 Allard, M. *et al.* TCR-ligand dissociation rate is a robust and stable biomarker of CD8+ T cell potency. *JCI Insight* **2**(2017). <https://doi.org/10.1172/jci.insight.92570>
- 13 Nauerth, M. *et al.* TCR-ligand koff rate correlates with the protective capacity of antigen-specific CD8+ T cells for adoptive transfer. *Sci Transl Med* **5** , 192ra187 (2013). <https://doi.org/10.1126/scitranslmed.3005958>
- 14 Nauerth, M. *et al.* Flow cytometry-based TCR-ligand Koff -rate assay for fast avidity screening of even very small antigen-specific T cell populations ex vivo. *Cytometry A* **89** , 816-825 (2016). <https://doi.org/10.1002/cyto.a.22933>
- 15 Purcarea, A. *et al.* Signatures of recent activation identify a circulating T cell compartment containing tumor-specific antigen receptors with high avidity. *Sci Immunol* **7** , eabm2077 (2022). <https://doi.org/10.1126/sciimmunol.abm2077>
- 16 Schober, K. *et al.* Reverse TCR repertoire evolution toward dominant low-affinity clones during chronic CMV infection. *Nat Immunol* **21** , 434-441 (2020). <https://doi.org/10.1038/s41590-020-0628-2>
- 17 Oliveira, G. *et al.* Phenotype, specificity and avidity of antitumour CD8(+) T cells in melanoma. *Nature* **596** , 119-125 (2021). <https://doi.org/10.1038/s41586-021-03704-y>
- 18 Straub, A. *et al.* Recruitment of epitope-specific T cell clones with a low-avidity threshold supports efficacy against mutational escape upon re-infection. *Immunity* **56** , 1269-1284 e1266 (2023). <https://doi.org/10.1016/j.immuni.2023.04.010>
- 19 Cai, C. *et al.* Identification of human progenitors of exhausted CD8(+) T cells associated with elevated IFN-gamma response in early phase of viral infection. *Nat Commun* **13** , 7543 (2022). <https://doi.org/10.1038/s41467-022-35281-7>
- 20 Cunningham, E. B. *et al.* Ongoing incident hepatitis C virus infection among people with a history of injecting drug use in an Australian prison setting, 2005-2014: The HITS-p study. *J Viral Hepat* **24** , 733-741 (2017). <https://doi.org/10.1111/jvh.12701>
- 21 Page-Shafer, K. *et al.* Testing strategy to identify cases of acute hepatitis C virus (HCV) infection and to project HCV incidence rates. *J Clin Microbiol* **46** , 499-506 (2008). <https://doi.org/10.1128/JCM.01229-07>
- 22 Eltahla, A. A. *et al.* Linking the T cell receptor to the single cell transcriptome in antigen-specific human T cells. *Immunol Cell Biol* **94** , 604-611 (2016). <https://doi.org/10.1038/icb.2016.16>
- 23 Hombrink, P. *et al.* Mixed functional characteristics correlating with TCR-ligand koff -rate of MHC-tetramer reactive T cells within the naive T-cell repertoire. *Eur J Immunol* **43** , 3038-3050 (2013). <https://doi.org/10.1002/eji.201343397>
- 24 Richard, A. C. *et al.* T cell cytolytic capacity is independent of initial stimulation strength. *Nat Immunol* **19** , 849-858 (2018). <https://doi.org/10.1038/s41590-018-0160-9>
- 25 Geginat, J., Lanzavecchia, A. & Sallusto, F. Proliferation and differentiation potential of human CD8+ memory T-cell subsets in response to antigen or homeostatic cytokines. *Blood* **101** , 4260-4266 (2003). <https://doi.org/10.1182/blood-2002-11-3577>
- 26 Day, E. K. *et al.* Rapid CD8+ T cell repertoire focusing and selection of high-affinity clones into memory following primary infection with a persistent human virus: human cytomegalovirus. *J Immunol* **179** , 3203-3213 (2007). <https://doi.org/10.4049/jimmunol.179.5.3203>
- 27 Knudson, K. M., Goplen, N. P., Cunningham, C. A., Daniels, M. A. & Teixeira, E. Low-affinity T cells are programmed to maintain normal primary responses but are impaired in their recall to low-affinity ligands. *Cell Rep* **4** , 554-565 (2013). <https://doi.org/10.1016/j.celrep.2013.07.008>

- 28 Zehn, D., Lee, S. Y. & Bevan, M. J. Complete but curtailed T-cell response to very low-affinity antigen. *Nature* **458** , 211-214 (2009). <https://doi.org/10.1038/nature07657>
- 29 Solouki, S. *et al.* TCR Signal Strength and Antigen Affinity Regulate CD8(+) Memory T Cells. *J Immunol* **205** , 1217-1227 (2020). <https://doi.org/10.4049/jimmunol.1901167>
- 30 Martinez, R. J. & Evavold, B. D. Lower Affinity T Cells are Critical Components and Active Participants of the Immune Response. *Front Immunol* **6** , 468 (2015). <https://doi.org/10.3389/fimmu.2015.00468>
- 31 Abdel-Hakeem, M. S., Bedard, N., Murphy, D., Bruneau, J. & Shoukry, N. H. Signatures of protective memory immune responses during hepatitis C virus reinfection. *Gastroenterology* **147** , 870-881 e878 (2014). <https://doi.org/10.1053/j.gastro.2014.07.005>
- 32 Luxenburger, H., Neumann-Haefelin, C., Thimme, R. & Boettler, T. HCV-Specific T Cell Responses During and After Chronic HCV Infection. *Viruses* **10** (2018). <https://doi.org/10.3390/v10110645>
- 33 Tschärke, D. C., Croft, N. P., Doherty, P. C. & La Gruta, N. L. Sizing up the key determinants of the CD8(+) T cell response. *Nat Rev Immunol* **15** , 705-716 (2015). <https://doi.org/10.1038/nri3905>
- 34 Liddy, N. *et al.* Monoclonal TCR-redirectioned tumor cell killing. *Nat Med* **18** , 980-987 (2012). <https://doi.org/10.1038/nm.2764>
- 35 Picelli, S. *et al.* Smart-seq2 for sensitive full-length transcriptome profiling in single cells. *Nature Methods* **10** , 1096-1098 (2013). <https://doi.org/10.1038/nmeth.2639>
- 36 Picelli, S. *et al.* Full-length RNA-seq from single cells using Smart-seq2. *Nature Protocols* **9** , 171-181 (2014). <https://doi.org/10.1038/nprot.2014.006>
- 37 Wang, G. C., Dash, P., McCullers, J. A., Doherty, P. C. & Thomas, P. G. T cell receptor alpha diversity inversely correlates with pathogen-specific antibody levels in human cytomegalovirus infection. *Sci Transl Med* **4** , 128ra142 (2012). <https://doi.org/10.1126/scitranslmed.3003647>

FIGURES

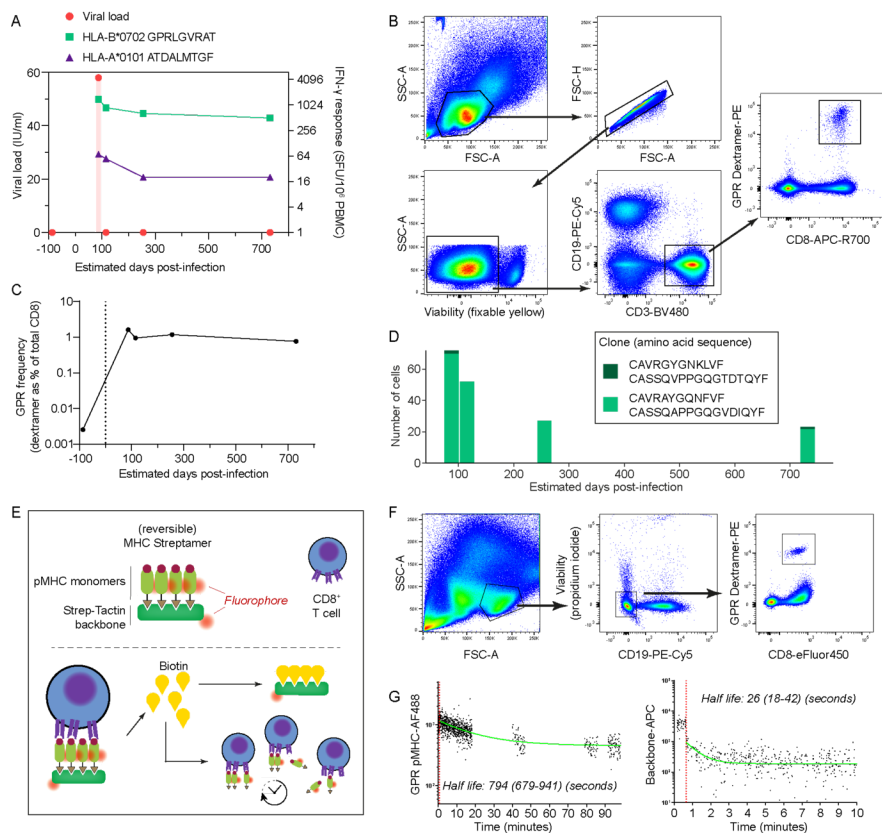


Figure 1. A monoclonal, high affinity CD8⁺ T cell population generated following natural HCV infection.

A. Longitudinal measurements of viral load and IFN- γ ELISpot responses to two HCV-derived CD8⁺ T cell epitopes in CL-MCRL. IU: international units. SFU: spot-forming units. B. Representative flow cytometry gating for Dextramer staining of HCV-specific CD8⁺ T cells. C. Frequency of cells specific for the GPR-epitope measured by Dextramer staining in CL-MCRL. D. Stacked bar plot showing the diversity of GPR-specific clonotypes with paired CDR3 α and CDR3 β amino acid sequences at time points from CL-MCRL. E. Schematic of the k_{off} dissociation assay using reversible Streptamers. pMHC: peptide-MHC. F. Flow cytometry gating for the identification of the GPR-specific population for the k_{off} dissociation assay. G. Dot plot of staining intensity of the reversible Streptamer backbone and pMHC components over time. The dotted red line indicates the time of addition of biotin. The green curve shows the non-linear regression. The half-life of the curve was calculated and numbers in brackets represent 95% confidence intervals. Cells were placed on ice during intervening periods.

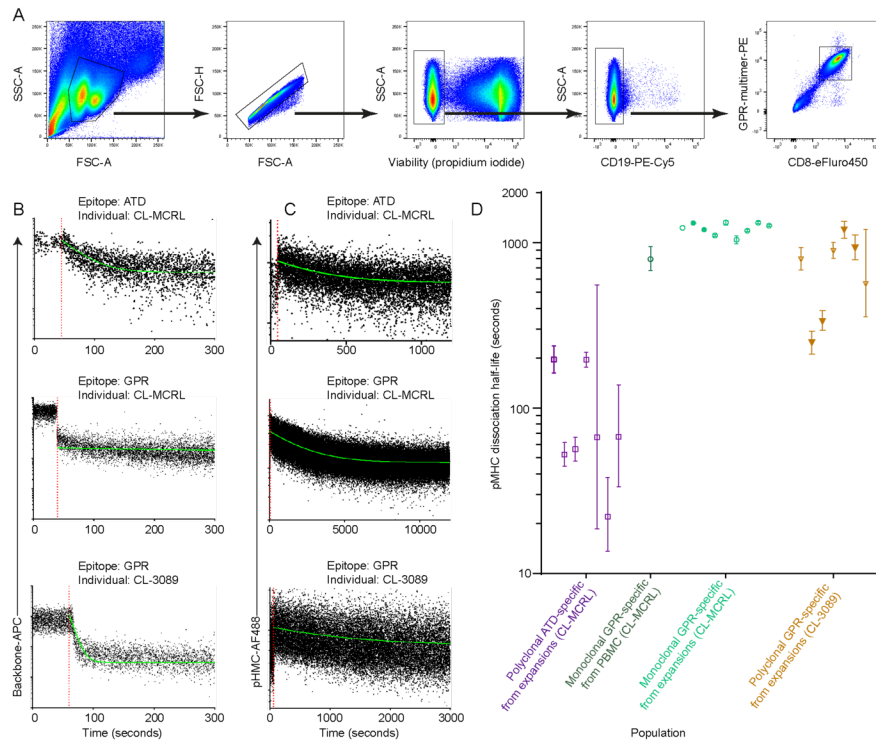


Figure 2. Comparative HCV-specific clonotypes from polyclonal populations are lower affinity than the monoclonal clonotype.

A. Representative flow cytometry gating for HCV-specific CD8⁺ T cell colonies stained with non-reversible multimers. B. Representative dots plots of fluorescence intensity from the reversible Streptamer backbone during the k_{off} dissociation assay of single cell colony expansions. C. Representative dots plots of fluorescence intensity from the reversible Streptamer pMHC during the k_{off} dissociation assay of single cell colony expansions. D. Box and whiskers plots of dissociation half-life times of all measured clonotypes. Whiskers represent 95% confidence intervals from non-linear regression. Pairs of solid colored symbols show cells derived from the same colony expansion but cryopreserved and dissociations measured independently.

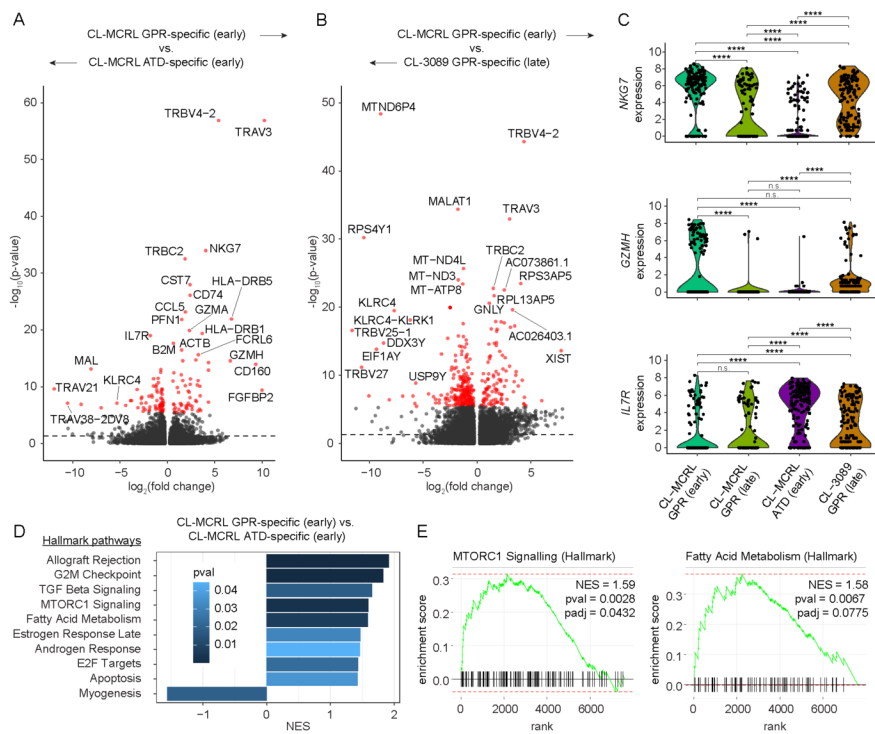
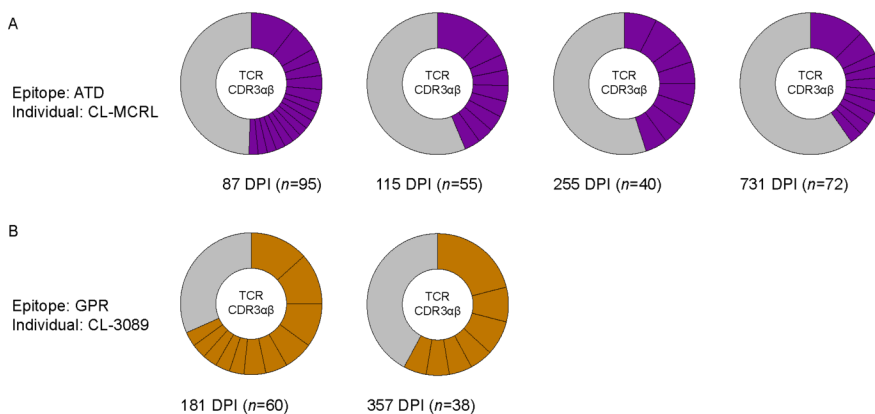


Figure 3. The monoclonal GPR-specific response is characterised by effector signatures.

A. Volcano plot of differentially expressed genes between GPR- and ATD-specific populations from CL-MCRL. Dashed line indicates p -value < 0.05 . Genes highlighted in red indicate adjusted p -values corrected by Bonferroni correction < 0.05 . B. Volcano plot of differentially expressed genes between GPR-specific populations from CL-MCRL and CL-3089 calculated using Mann-Whitney U test. Dashed line indicates p -value < 0.05 . Genes highlighted in red indicate adjusted p -values corrected by Bonferroni correction < 0.05 . C. Violin plots showing the transcriptional expression level of effector-associated markers. D. GSEA summary of differentially expressed genes between GPR- and ATD-specific populations from CL-MCRL, using the set of Hallmark pathways from the Human MSigDB collections. E. GSEA plot showing selected enriched pathways between GPR- and ATD-specific populations from CL-MCRL. NES: normalised enrichment score, p val: p -value, $padj$: adjusted p -value. Statistical significance was determined by Mann-Whitney U test (A and B) and Broad GSEA test (D and E). n.s. not significant, **** $p < 0.0001$



Supplementary figure 1. Polyclonal repertoires of comparative HCV-specific CD8+ T cell populations.

A. Pie charts of the distribution of ATD-specific clonotypes (paired CDR3 α and CDR3 β amino acid) from CL-MCRL recovered by single-cell RNA-sequencing. B. Pie charts of the distribution of GPR-specific clonotypes (paired CDR3 α and CDR3 β amino acid) from CL-3089 recovered by single-cell RNA-sequencing. DPI: days post-infection. Colored segments represents a unique expanded clonotypes and grey segments represent all singleton clonotypes.

TABLES

Table 1 . Subjects details.

Subject	Gender	Age at infection	Infecting virus genotype	Epitope	Protein source
CL-3089	M	26	1b	HLA-B*0702 GPRLGVRAT	CORE (41-49)
CL-MCRL	F	25	1a	HLA-B*0702 GPRLGVRAT	CORE (41-49)
CL-MCRL	F	25	1a	HLA-A*0101 ATDALMTGF	NS3 (1436-1444)

DPI: days post-infection

Table 2: Single cell colonies and affinity for T-cell receptors specific for HLA-A*0101 ATDALMTGF.

Subject	Colony	Half-life (sec)	95% CI (sec)	k_{off} constant	95 % CI k_{off}	V gene
CL-MCRL	CL-D1/D2-4	195.8	163-237.2	3.54E-03	2.92E-03 to 4.25E-03	
CL-MCRL	CL-C1-2	52.41	44.5-61.9	1.32E-02	1.12E-02 to 1.56E-02	TRAV8-4*03; TR
CL-MCRL	CL-C1-6	56.33	47.8-66.5	1.23E-02	1.04E-02 to 1.45E-02	TRAV21*01; TR
CL-MCRL	CL-D1/D2-38	195.6	177.7-216.4	3.54E-03	3.20E-03 to 3.90E-03	TRAV38-2/ DV8
CL-MCRL	CL-A1/A2-16	66.41	18.6-555.3	1.04E-02	1.25E-03 to 3.73E-02	TRAV3*01
CL-MCRL	CL-C1-7	22.07	13.6-37.9	3.14E-02	1.83E-02 to 5.10E-02	TRAV8-3*01; TR
CL-MCRL	CL-B1-12	67.12	33.4-138.3	1.03E-02	5.01E-03 to 2.08E-02	TRAV8-4*07

Table 3 . Single cell colonies and affinity for T-cell receptors specific for HLA-B*0702 GPRLGVRAT.

Subject	Colony	Half-life (sec)	95% CI (sec)	k_{off} constant	95 % CI k_{off}	V gene
CL-MCRL	CL-P1-1A*	1311	1299-1323	5.29E-04	5.24E-04 to 5.34E-04	
CL-MCRL	CL-P1-1B*	1194	1174-1215	5.81E-04	5.70E-04 to 5.90E-04	
CL-MCRL	CL-P1-6B	1228	1207-1249	5.64E-04	5.55E-04 to 5.74E-04	
CL-MCRL	CL-P2-1B	1104	1089-1120	6.28E-04	6.19E-04 to 6.36E-04	
CL-MCRL	CL-P2-5B	1321	1285-1360	5.25E-04	5.10E-04 to 5.39E-04	
CL-MCRL	CL-P2-7B	1039	985-1097	6.67E-04	6.32E-04 to 7.04E-04	
CL-MCRL	CL-P2-9B	1180	1160-1201	5.87E-04	5.77E-04 to 5.98E-04	
CL-MCRL	CL-P1-11B	1319	1294-1346	5.26E-04	5.15E-04 to 5.36E-04	
CL-MCRL	CL-P1-21	1263	1247-1279	5.49E-04	5.42E-04 to 5.56E-04	
CL-MCRL	Monoclonal from PBMC	794	679-941	8.73E-04	7.37E-04 to 1.02E-03	TRAV
CL-3089	D7	790	681-934	8.77E-04	7.42E-04 to 1.02E-03	TRAV
CL-3089	E6*	333	295-378	2.08E-03	1.83E-03 to 2.35E-03	TRAV
CL-3089	E6-2*	247	212-291	2.81E-03	2.38E-03 to 3.27E-03	As abc
CL-3089	F3	891	803-998	7.78E-04	6.95E-04 to 8.63E-04	TRAV
CL-3089	F4*	926	789-1111	7.49E-04	6.24E-04 to 8.79E-04	TRAV
CL-3089	F4-2*	1191	1065-1345	5.82E-04	5.15E-04 to 6.51E-04	As abc

Subject	Colony	Half-life (sec)	95% CI (sec)	k_{off} constant	95 % CI k_{off}	V gen
CL-3089	CL10-060417	563	356-1197	1.23E-03	5.79E-04 to 1.95E-03	

Figure 1

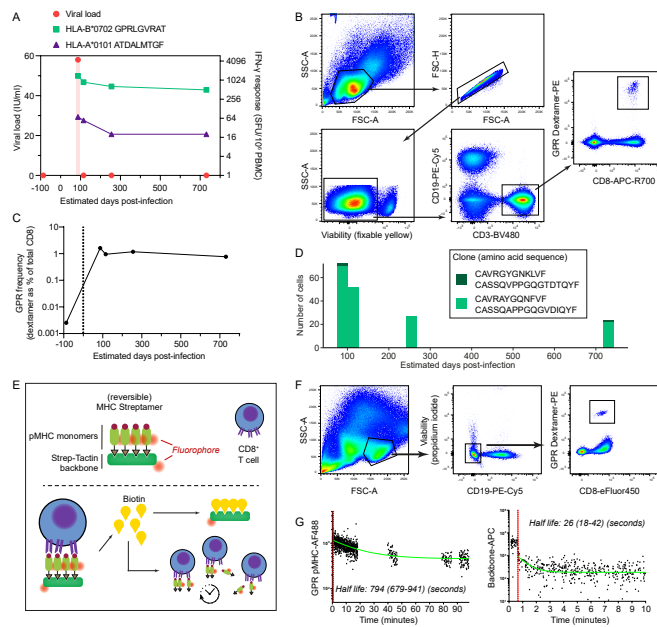


Figure 2

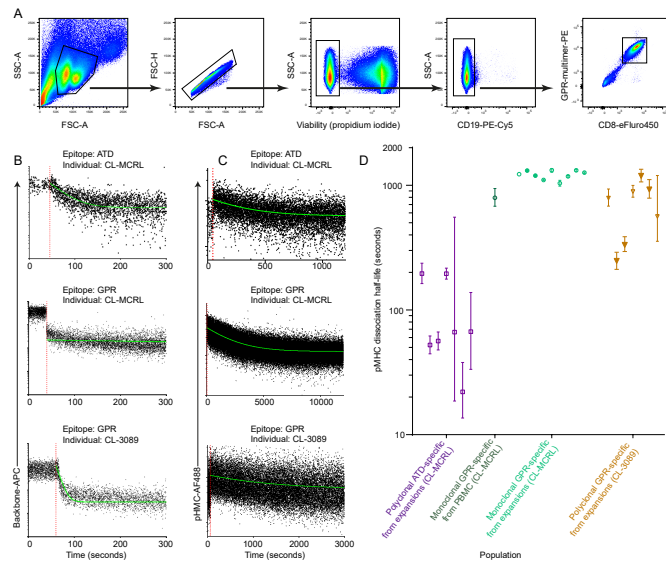


Figure 3

